Numerical analysis of multi-photon parameters from ultrafast laser measurements

M. J. Potasek[*a,b] and E. Parilov[a]

[a]Simphotek, Inc., 211 Warren St., Newark, NJ 07103

[b]Courant Institute of Mathematical Sciences, New York University, N.Y.

ABSTRACT

We describe a unique mathematical/numerical model to analyze ultrafast laser experimental data and obtain two-photon (TPA) and multi-photon (MPA) absorption parameter(s). The material used to demonstrate the numerical method is a hybrid organic-inorganic nano-structured semiconductor quantum dot-polymer composite. Chemical, biological and engineering studies require advancements in TPA/MPA absorbers for microscopy, fluorescence, imaging, and micro-processing of materials. We illustrate the numerical method by fitting data from the well-known z-scan experimental method. Often an analytical model is used to analyze data from such experiments, which is limited in scope with certain restrictions on laser intensity and material thickness.

A more general mathematical/numerical method that includes TPA/MPA and can be extended to free carrier absorption and stimulated emission is described. Under certain circumstances, we can also calculate the electron population density on every electronic level to demonstrate physical effects such as saturation. Additionally, we include diffraction in our numerical calculation so that the TPA/MPA can be obtained even for thick optical samples. We use the numerical method to calculate published z-scan measurements on quantum-dot CdS-polymer composites, and show excellent agreement with published analytical results.

Keywords: ultrashort pulses, multi-photon absorption, numerical calculation, semiconductor quantum dots, z-scan

1. INTRODUCTION

We extend and demonstrate our optical building block/transition module methodology: a computational Lego-like system for describing existing and/or composing novel energy level diagrams and for building a mathematical model (numerical algorithm) of ultrashort laser interaction with semiconductor quantum dot materials. The method uses (computational) transition modules (TMs) or optical building blocks describing electronic transitions between different energy levels as well as the levels' absorption/relaxation parameters that are linked to matrices and vectors in coupled equations of the mathematical model. This approach enables modification so that new energy levels and their corresponding equations with photophysical parameters can be added or deleted directly on the user interface without rewriting the numerical program. Combined, they allow one to optimize design functionalities and parameters of a significant variety of photoactive materials, without repeated material synthesis, measurements, or numerical coding.

Materials of nanometer dimensions[1-3] have attracted significant attention in several areas such as, physics, chemistry, and biology for their unique chemical and physical properties in addition to their potential technological applications mentioned below. These capabilities are mainly due to the unusual dependence of the electronic and optical properties (such as linear and nonlinear absorption) on quantum confinement, which for semiconductor materials restricts the particle size in the 1 to 10 nm range.

In particular, semiconductor quantum dots (QD) have many desirable properties that are well suited for nonlinear materials, lasers, detectors, imaging agents, solar energy conversion and biomedical diagnostics. Amongst the many types of QDs are those made of II-VI and III-V semiconductors such as, CdS, CdSe, PbS, InP, and GaAs. Many theoretical/numerical analyses of optical properties of QDs neglect laser propagation effects or do not treat them completely. In this example we describe the incorporation of various QD absorption and relaxation mechanisms, which significantly enhances the QD analysis/design.

[*]mpotasek@simphotek.com, phone 1 973 621 2340

2. SEMICONDUCTOR QUANTUM DOTS

Semiconductor quantum dots (QDs) are often referred to as artificial atoms, which consist of hundreds to thousands of atoms. A few reviews of the synthesis, structure and properties of nanomaterials are given the references[4,5] As a result of the quantum confinement, QDs exhibit unique physical and optical properties that are not present in bulk material. A QD is a quasi-zero-dimensional object where the carrier movement is restricted in three dimensions. The bulk crystalline structure of the semiconductor is maintained in the QD, but they have atomic-like discrete energy states due to 3D confinement.[1]
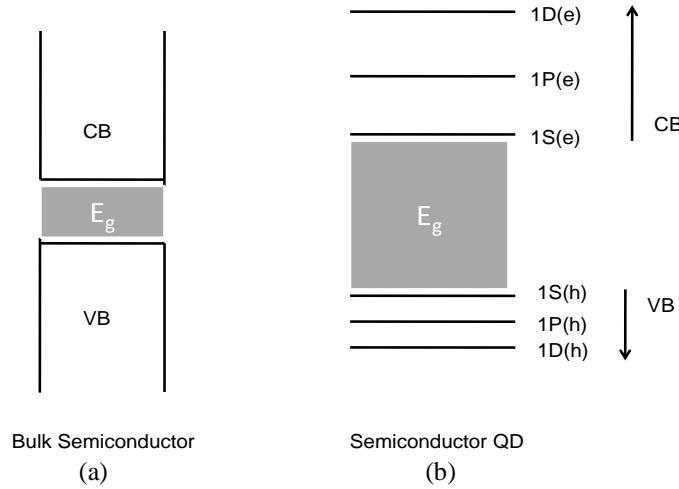
Fig. 1. Energy level diagrams. (a) bulk semiconductor (b) quantum dot assuming single valence bands.

Typically the effective-mass model is used to describe the electronic structure of QDs[6]. In this description, electron states are annotated by using a letter (l) to denote the angular momentum of the envelop wave functions. Using spectroscopic notation, the following symbols are used S for l=0, P for l=1, D for l=2, etc. The degeneracy of the electron states are $2(2l+1)$-fold degenerate and the lowest three electron states are denoted by 1S, 1P, 1D. The hole states are generally more complicated than shown in the figure above and are labeled similarly to electron states with an additional subscript for the total hole angular momentum (j), which have a degeneracy of $2j+1$. The first three hole states are $1S_{3/2}, 1P_{3/2}, 2S_{3/2}$. The interband selection rules allow for transitions from $nS_j(h)$ hole states to all $S(e)$ electron states, $nP_j(h)$ hole states to all $P(e)$ electron states, etc. where n is the ordinal number of the level. A schematic diagram is given in the figure below.
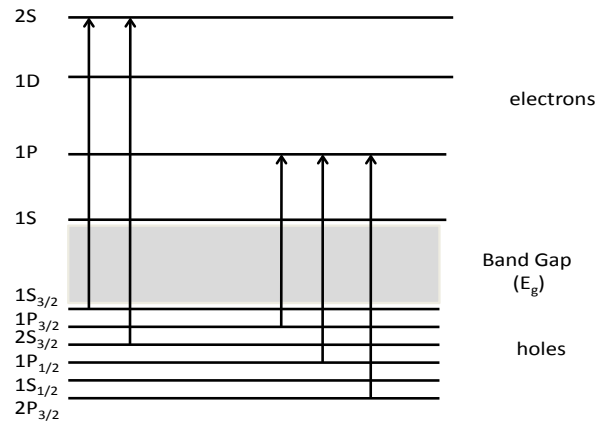

Fig. 2. Energy level diagram and transitions for semiconductor quantum dot.

The above figure shows five absorptive transitions of a single photon from states $1S_{3/2}$ to 2S; $2S_{3/2}$ to 2S; $1P_{3/2}$ to 1P; $1P_{1/2}$ to 1P and $1S_{1/2}$ to 1P.   The energies of the excitons depend on the relative energies of the electron and hole states. The energies of the exciton transitions may be obtained from spectroscopic measurements. Often these spectroscopic measurements are compared to theoretical calculations of the electron and hole energy levels.

There are several generation/recombination processes in semiconductors[1,7,8]. Excitons are created by single or multiphoton absorption, free carrier absorption, and impact ionization (bi-exciton). Relaxation of excitons can occur by phonon (intraband), spontaneous or stimulated radiative (interband) and Auger transitions. The Auger process is non-radiative and is mediated by electron-electron (e-e) Coulomb interactions. The decay of multi-electron levels is dominated by Auger processes. QDs have a large surface to volume ratio that leads to trap states in the band gap (not shown). In many QDs the surface states are passivated by capping the QD.

3. THEORETICAL AND NUMERICAL METHOD

We describe a laser (electromagnetic field) interacting with a QD (energy levels as described in Figs. 1 and 2) with absorption and relaxation mechanisms described in Section 2. This involves a set of coupled equations for the field and the rate equations for the QD.

The propagation of the electromagnetic wave is given by the scalar Maxwell equation given below.

$$\nabla^2 E(z,r,t) - \frac{1}{c^2}\frac{\partial^2}{\partial t^2}E(z,r,t) = \frac{1}{\varepsilon_0 c^2}\frac{\partial^2}{\partial t^2}P(z,r,t), \tag{1}$$

where E is the optical field, P is the induced nonlinear polarization and ω_0 (k_0) is the frequency (wave number) of the incident electromagnetic field. The density matrix operator for the nonlinear material is defined as $\hat{\rho} = |\psi\rangle\langle\psi|$, and the equation of motion is

$$\frac{\partial \rho_{jk}}{\partial t} = \frac{-i}{\hbar}\sum_l \left(H_{jl}\rho_{lk} - \rho_{kl}H_{lj}\right), \tag{2}$$

where the matrix elements ρ_{jk} correspond to a polarization induced by a transition between energy levels j and k, $|\psi\rangle$ is the wavefunction and H is the Hamiltonian. Equation (2) gives rise to the rate equations, a set of coupled partial differential equations describing the energy levels and the transitions between them. Previously, Parilov and Potasek[9-11] derived a method of writing the rate equations in terms of matrix and vector equations, which coupled to Eq. (1) were solved numerically to determine the propagating field and the population dynamics.   Using this mathematical description, Parilov and Potasek defined a set of abstract diagrams[9-12] (computational building blocks or Transition Modules-TM) uniquely linked to each matrix.   Distinct matrices were defined for absorption and relaxation mechanisms and every photo-physical parameter was uniquely linked to a specific element in its defined matrix. Photo-physical parameters were also linked to the laser propagation equation written in a matrix-vector format.   This technique enables one to create matrices and vectors combining the parameters of multiple energy levels and photo-transitions.   Since it does not rely on solving nonlinear partial differential equations, the number of energy levels, absorptions and relaxations involved is (nearly) unlimited and set up in real-time. This technique allows one to set up and modify the equations without reprogramming them.

The following are the schematic diagrams of absorption blocks with absorption of α photons. The diagrams specify energy levels involved in the absorption and the molar cross section parameter $\sigma_{[\alpha]PA}^{s_1 s_2}$, followed by the *block's diagram expressions* for the absorption block denoted by $^m A_{s_1 s_2}^{\alpha}$ and the second type of basic TM a *relaxation (transition) block*,

denoted by ${}^{m_1 m_2}\mathrm{R}{}_{s_1 s_2}^{\text{type}}$, which represents electron/exciton/phonon relaxations where the subscripts/superscripts are defined in Fig. 3.
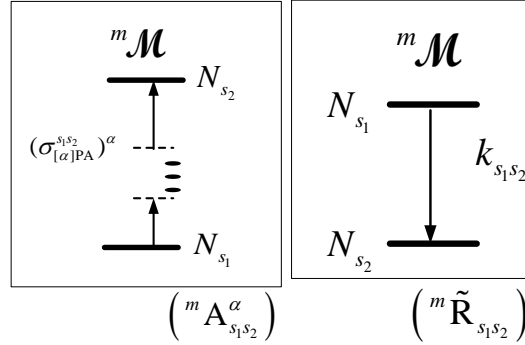

Fig. 3. Absorption TM (left side) and Relaxation TM (right side).

Under the TM framework, every transition block describes one transition within the energy level diagram of the material and relates certain algebraic terms in the corresponding system of coupled PDEs[9-12]. The coupled equations are given by[9-12]

$$
\begin{cases}
\dfrac{\partial \mathbf{N}(\eta,\rho,\tau)}{\partial \tau} = \left[d_0 \mathbf{D}_0 + \sum_{\alpha=1}^{N_A} d_\alpha \mathbf{D}_\alpha \overline{Q}^\alpha(\eta,\rho,\tau) \right] \mathbf{N}(\eta,\rho,\tau) \\[2mm]
\dfrac{\partial Q(\eta,\rho,\tau)}{\partial \eta} = \left[-\sum_{\beta=1}^{N_B} g_\beta \big(\boldsymbol{\sigma}_\beta \cdot \mathbf{N}(\eta,\rho,\tau) \big) \overline{Q}^{\beta-1}(\eta,\rho,\tau) + \dfrac{i}{4}\nabla_\rho^2 - c_L \right] Q(\eta,\rho,\tau)
\end{cases}
\tag{3}
$$

where $\mathbf{N}$ is normalized vectors of population densities to be sought, I_0 is the peak intensity, $\overline{Q}(\eta,\rho,\tau) = Q(\eta,\rho,\tau)Q^*(\eta,\rho,\tau)$, $Q(\eta,\rho,\tau)$ is a complex normalized electromagnetic field to be sought given at depth η, ρ and τ are normalized radius and time, respectively [$Q(\eta=0,\rho,\tau) = e^{-(\tau')^2/2} e^{-(\rho')^2/2}$ is a normalized incident electromagnetic field], N is the molecular concentration, $L_{df} = \pi R_0^2 n_0 / \lambda$ is the diffraction length, $\tilde{c}$ is the linear absorption, $\mathbf{D}_0$ are constant matrices of decay rates $k_{s_2 s_1}$, $\mathbf{D}_\alpha$ are matrices for the molar absorption cross-sections $\sigma_{s_1 s_2}^{[\alpha]PA}$, $\boldsymbol{\sigma}_\beta \left(\left\{ \sigma_{s_1 s_2}^{[\beta]PA} \right\} \right)$ are constant S-dimensional vectors and $\dfrac{i}{4}\nabla_\rho^2$ is the diffraction operator. The constants d_α, g_β, and c_L are introduced to absorb all the multiplication factors under single constants and are given by $d_0 = T_0$, $d_\alpha = \dfrac{T_0 I_0^\alpha}{\alpha \hbar \omega_0}$, $g_\beta = -L_{df} N I_0^{\beta-1}$, $c_L = \tilde{c} L_{df}$. Further details of the normalized equations are given in refs. 10 and 11. Except for rarely-used simple cases, an analytic solution for the beam propagation Eq. (3) cannot be obtained. Finding a robust numerical solution for these equations also requires applying non-trivial numerical schemes. Our numerical solution is based on a finite difference split-step method enhanced by the Crank-Nicholson integration technique. Below we will describe just the essence of our numerical scheme, i.e. the propagation of the electric field by a small step. We apply the beam propagation method, where details are presented in refs.10 and 11, An approximate solution at the step $\eta + \Delta\eta$, given a solution at η, is given by

$$
\mathbf{N}(\tau + \Delta\tau) \approx \exp\left(\int_\tau^{\tau+\Delta\tau} \Upsilon_{\text{rate}}(\eta,\rho,\tau')\, d\tau' \right) \circ \mathbf{N}(\tau) ,
\tag{4}
$$

$$Q(\eta + \Delta\eta) \approx \exp\left(\int_{\eta}^{\eta+\Delta\eta} \Phi_{\text{rate}}(\eta', \rho, \tau) + \Psi_{\text{df}}(\eta', \rho, \tau)\, d\eta' \right) \circ Q(\eta).$$

Φ_{rate} does not commute with Ψ_{df}; therefore, to resolve the summation in the exponent, we apply the split-step method as follows:

$$Q(\eta + \Delta\eta) \approx e^{\frac{\Delta\eta}{2} \Psi_{\text{df}}(\rho, \tau)} \circ \exp\left(\int_{\eta}^{\eta+\Delta\eta} \Phi_{\text{rate}}(\eta', \rho, \tau)\, d\eta' \right) \circ e^{\frac{\Delta\eta}{2} \Psi_{\text{df}}(\rho, \tau)} \tag{5}$$

We apply Crank-Nicholson method to exponential terms in Equations. (4)-(5) to make the numerical integration more robust.

$$\mathbf{N}(\tau + \Delta\tau) \approx \exp\left(\int_{\tau}^{\tau+\Delta\tau} \Upsilon_{\text{rate}}(\eta, \rho, \tau')\, d\tau' \right) \circ \mathbf{N}(\tau)$$

$$\approx \exp\left(\Delta\tau \Upsilon_0 \right) \prod_{\alpha=1}^{N_A} \exp\left(\Delta\tau \left\{ \frac{\Upsilon_\alpha^Q(\eta - \Delta\eta/2) + \Upsilon_\alpha^Q(\eta + \Delta\eta/2)}{2} \right\} \right) \mathbf{N}(\tau) \ . \tag{6}$$
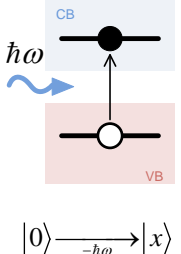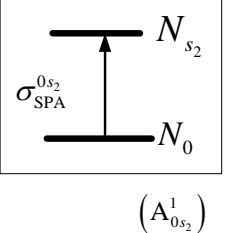
$$Q(\eta + \Delta\eta) \approx \exp\left(\frac{\Delta\eta}{2} \left\{ \frac{\Psi_{\text{df}}(\eta) + \Psi_{\text{df}}(\eta + \Delta\eta)}{2} \right\} \right) \circ \exp\left(\Delta\eta\, \Phi_c \right)$$
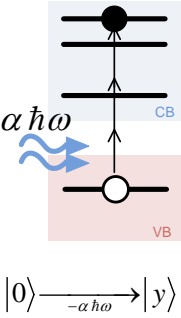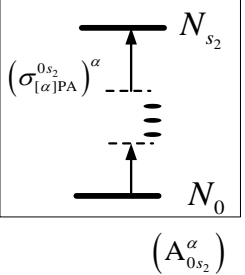
$$\times \prod_{\beta=1}^{N_B} \exp\left(\Delta\eta \left\{ \frac{\Phi_\beta^N(\tau - \Delta\tau/2) + \Phi_\beta^N(\tau + \Delta\tau/2)}{2} \right. \right.$$

$$\left. \left. \times \left\{ \frac{\Phi_\beta^Q(\eta) + \Phi_\beta^Q(\eta + \Delta\eta)}{2} \right\} \right\} \right) \exp\left(\frac{\Delta\eta}{2} \left\{ \frac{\Psi_{\text{df}}(\eta) + \Psi_{\text{df}}(\eta + \Delta\eta)}{2} \right\} \right) \circ Q(\eta) \tag{7}$$
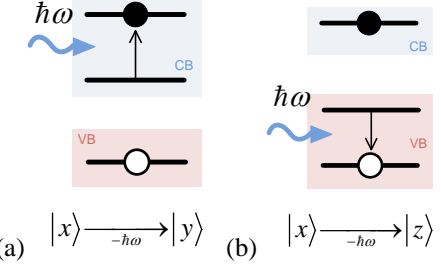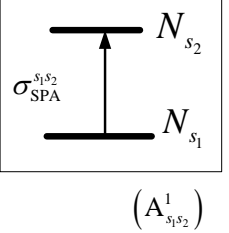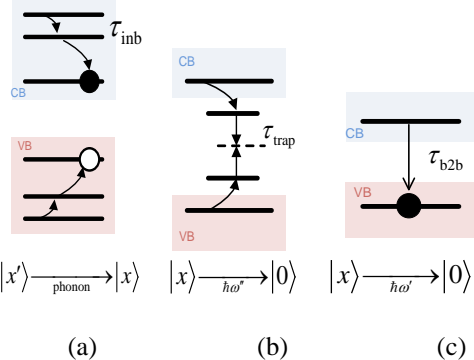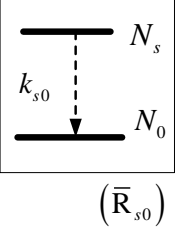
Using these methods, it is feasible to solve numerically the above beam propagation equations, which includes the diffraction term.
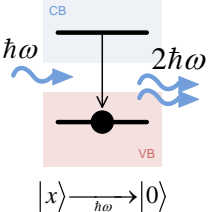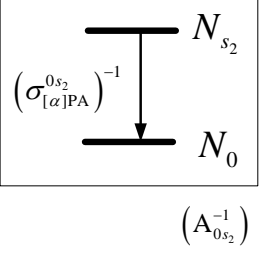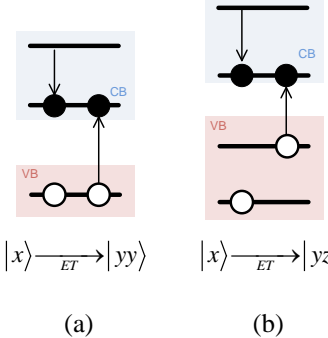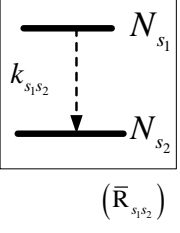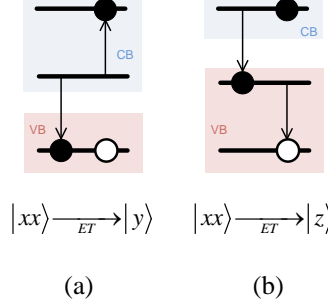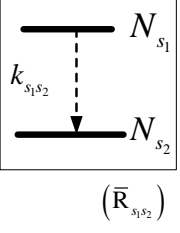
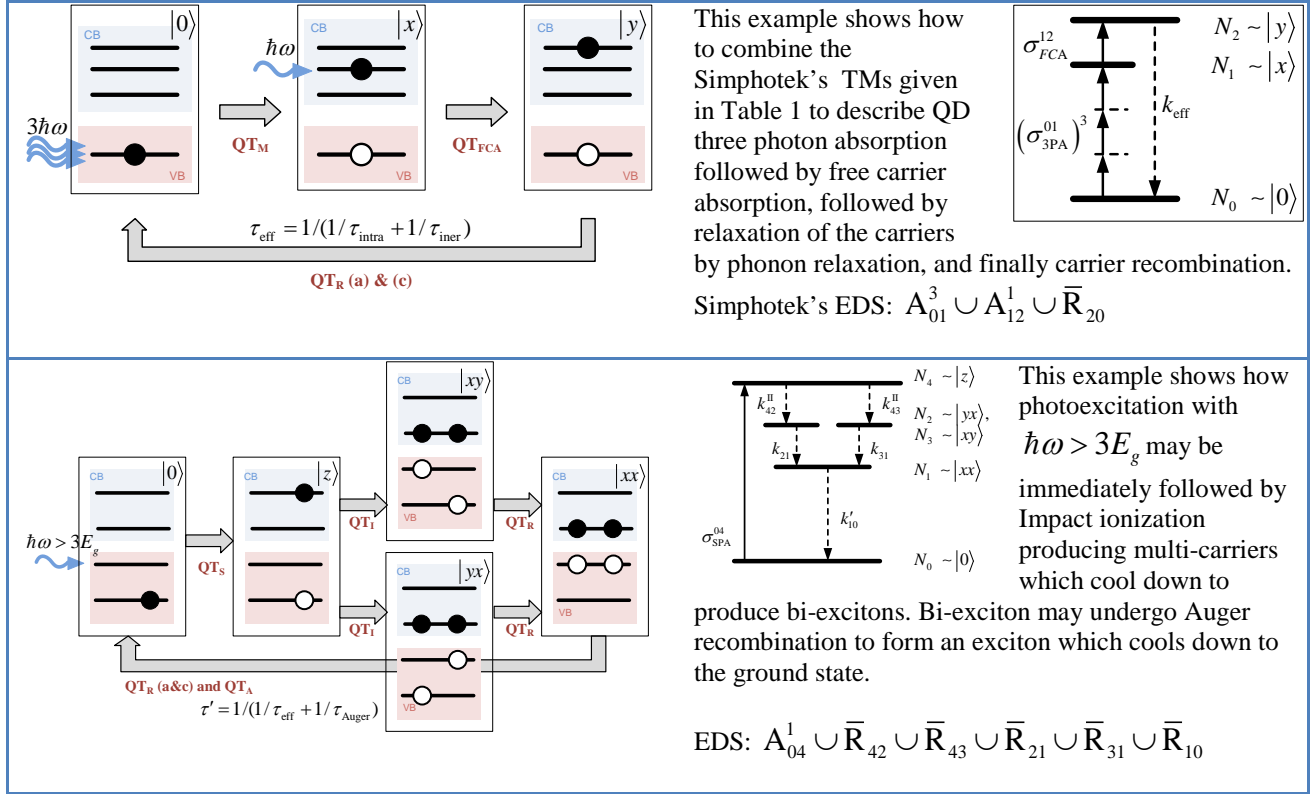## 4. DESCRIPTION OF TRANSITIONS AND TRANSITION MODULES

In Table 1 we provide a description of energy transitions and diagrams of the transition modules.

Table 1. QD energy transitions, descriptions and TM.

QD energy transition type	Transition description (with labels)	TM
Single-exciton formation (by SPA) A single photon is absorbed by an electron in the valence band. The negatively charged electron is excited to the conduction band, leaving a positively-charged hole in the valence band: $E_{\text{photon}} > E_{\text{gap}}$	$\hbar\omega$ $\;$ $\lvert 0 \rangle$ is ground state; $\lvert x \rangle$ is single-exciton state; Energy requirement: $E_{\lvert x \rangle} = \hbar\omega$ $\lvert 0 \rangle \xrightarrow{-\hbar\omega} \lvert x \rangle$	$\sigma_{\text{SPA}}^{0s_2}$ $\;$ N_{s_2} $\;$ N_0 $\left(A_{0s_2}^1 \right)$ $N_0 \to \lvert 0 \rangle$ and $N_{s_2} \to \lvert x \rangle$

Single-exciton formation (by MPA) Two or more photons are absorbed simultaneously by an electron in the valence band. The negatively charged electron is excited to the conduction band, leaving a positively-charged hole in the valence band. For example: See ref. 13.	 $\alpha\hbar\omega$ $\lvert 0\rangle \xrightarrow{-\alpha\hbar\omega} \lvert y\rangle$	$\lvert y\rangle$ is single-exciton state; Energy requirement: $E_{\lvert y\rangle} = \alpha\hbar\omega$; $\alpha > 1$	 $\left(A_{0s_2}^{\alpha}\right)$ $N_0 \rightarrow \lvert 0\rangle$ and $N_{s_2} \rightarrow \lvert y\rangle$
Free carrier absorption (by SPA) An electron (hole) in the conduction (valence) band state absorbs a single photon (SPA) and is promoted to a higher energy state in the conduction (valence) band For example: See ref. 14.	 (a) $\lvert x\rangle \xrightarrow{-\hbar\omega} \lvert y\rangle$ (b) $\lvert x\rangle \xrightarrow{-\hbar\omega} \lvert z\rangle$	$\sigma_{SPA}^{s_1 s_2}$ $\left(A_{s_1 s_2}^{1}\right)$ $N_{s_1} \rightarrow \lvert x\rangle$ and $N_{s_2} \rightarrow \lvert y\rangle$; hole excitation is with $N_{s_2} \rightarrow \lvert z\rangle$
Excitation relaxation/recombination **(by phonon or photon)** Three cases: (a) Electron (hole) intraband transitions to lower states, by emitting phonons; (b) Electron and hole recombine in a trap state within the band gap by emitting a photon of longer wavelength; (c) Interband recombination of electron with its hole by emitting a photon. For example: See ref. 15	 $\lvert x'\rangle \xrightarrow{phonon} \lvert x\rangle$ $\lvert x\rangle \xrightarrow{\hbar\omega''} \lvert 0\rangle$ $\lvert x\rangle \xrightarrow{\hbar\omega'} \lvert 0\rangle$ (a) (b) (c)	k_{s0} N_s N_0 $\left(\bar{R}_{s0}\right)$ (a) These transitions are usually fast (sub-ps), so that we do not designate a TB but rather make them as a part of another, more significant transitions, like the lowest carrier state exciton recombination; (b) $N_s \rightarrow \lvert x\rangle$ and $N_0 \rightarrow \lvert 0\rangle$ $k_{s_1 s_2} = 1/\tau_A$ (c) the same way

Stimulated emission **(by SPA/MPA)** If population inversion exists, then an incoming photon may induce the emission of one or more photons. For example: See ref. 16	 $$E_{|x\rangle} = \hbar\omega$$ $$|x\rangle \xrightarrow{\hbar\omega} |0\rangle$$	 $$\left(\sigma^{0s_2}_{[\alpha]\text{PA}}\right)^{-1}$$ $$\left(A^{-1}_{0s_2}\right)$$ $N_s \rightarrow |x\rangle$ and $N_0 \rightarrow |0\rangle$
Impact ionization **(bi-excitons)** If a high-energy photon produces a single high-energy exciton that has a total energy greater than the energy of two low-energy excitons, then the high-energy exciton can decay to a low-energy exciton and simultaneously form a second low-energy exciton. This process conserves energy For example: See ref. 17	 $$|x\rangle \xrightarrow{ET} |yy\rangle \qquad |x\rangle \xrightarrow{ET} |yz\rangle$$ (a) (b)	 $$k_{s_1 s_2}$$ $$\left(\overline{R}_{s_1 s_2}\right)$$ Can be modeled by a non-radiative relaxation block. (a) $N_{s_1} \rightarrow |x\rangle$ and $N_{s_2} \rightarrow |yy\rangle$ (b) $N_{s_1} \rightarrow |x\rangle$ and $N_{s_2} \rightarrow |yz\rangle$
Auger **(bi-excitons)** Recombination of one electron-hole pair within a bi-exciton promoting the other electron-hole, either by exciting an electron (a) or a hole (b). QDs with more than two excitons can decay by consecutive Auger processes. For example: See ref.16.	 $$|xx\rangle \xrightarrow{ET} |y\rangle \qquad |xx\rangle \xrightarrow{ET} |z\rangle$$ (a) (b)	 $$k_{s_1 s_2}$$ $$\left(\overline{R}_{s_1 s_2}\right) \text{ Auger}$$ decay τ_A. $k_{s_1 s_2} = 1/\tau_A$ (a) $N_{s_1} \rightarrow |xx\rangle$ and $N_{s_2} \rightarrow |y\rangle$ (b) $N_{s_1} \rightarrow |xx\rangle$ and $N_{s_2} \rightarrow |z\rangle$
Examples		

This example shows how to combine the Simphotek's TMs given in Table 1 to describe QD three photon absorption followed by free carrier absorption, followed by relaxation of the carriers by phonon relaxation, and finally carrier recombination.

Simphotek's EDS: $A_{01}^3 \cup A_{12}^1 \cup \overline{R}_{20}$

This example shows how photoexcitation with $\hbar\omega > 3E_g$ may be immediately followed by Impact ionization producing multi-carriers which cool down to produce bi-excitons. Bi-exciton may undergo Auger recombination to form an exciton which cools down to the ground state.

EDS: $A_{04}^1 \cup \overline{R}_{42} \cup \overline{R}_{43} \cup \overline{R}_{21} \cup \overline{R}_{31} \cup \overline{R}_{10}$

5. Z-SCAN MEASUREMENT TECHNIQUE

A common experimental method for measuring the nonlinear properties of materials is the Z-scan measurement technique[18-21] where a single laser beam is tightly focused onto a nonlinear sample medium. The laser beam is directed perpendicular to the plane of the sample, which is moved along the z direction (the laser beam direction) in and out of the laser focal point. The transmitted signal goes either directly to a detector as shown in Fig. 4.
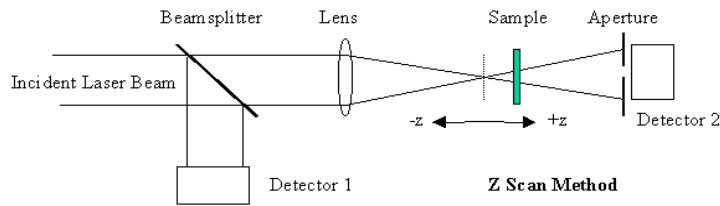
Fig. 4 Experimental arrangement for z-scan measurements. The solid straight line is z=0.

In this paper we concentrate on the open z-scan method so there is no aperture. A TEM$_{oo}$ Gaussian beam with a beam waist w_0 travelling along the +z-direction is assumed. The electric field is given by

$$E(r,z,t) = E_0(t)\frac{w_0}{w(z)}\exp\left(-\frac{r^2}{w^2(z)} - \frac{ikr^2}{2R(z)}\right)e^{-\phi(z,t)}, \qquad (5)$$

where $w^2(z) = w_0^2(1 + z^2/z_0^2)$ is the squared $1/e^2$ beam radius, $z_0 = k w_0^2/2$ is the diffraction length at z=0, R(z) is the radius of curvature, $E_0(t)$ contains the time dependence of the electric field. If the sample length is small compared to the diffraction length at z, then the medium is regarded as "thin" and diffraction can be neglected. We include both thin and thick materials. Previous authors have investigated various applications of thick samples. We approximate Eq. (5) using a Gaussian shaped function and neglect the phase term $\phi(z,t)$ such that

$$E(z,r,t) = \sqrt{I_{00}} \frac{w_0}{w(z)} \exp\left[-\frac{r^2}{w^2(z)}\right] \exp\left[-\frac{t^2}{T_0^2}\right]$$

(6)

where "at the focal point, z=0" w_0 is the $1/e^2$ of the radius, $T_0 = t_{FWHM}/2\sqrt{\ln 2}$, $R_0 = w_{HW1/e^2M}/\sqrt{2} = w_0/\sqrt{2}$,

$$I_{00} \approx \frac{E_{in}}{\pi\sqrt{\pi} R_0^2 T_0} .$$

6. APPLICATIONS

In this section we investigate four applications of the numerical method: (a) TPA in a thin film semiconductor QD material, (b) TPA in a semiconductor QD thick film material where diffraction must be taken into account, (c) two photon and excited state absorption in a Q-dot thin film, and (d) TPA with both spontaneous nonradiative emission and stimulated radiative two-photon emission. Except for the first two cases, the other cases cannot be calculated with traditional analytical expressions. Therefore our numerical method has several advantages over prior mathematical techniques.

6.1 Two-photon absorption in a surfactant-capped CdS QD material in a thin film.

We use our numerical method to investigate published z-scan results[26] for a surfactant-capped CdS QD in a thin film. The nonlinear optical properties were investigated with 25 ps laser pulses from a Nd:YAG laser at 532 nm. The beam waist was about 85 um at z=0. The schematic diagram is shown in Fig. 4. Table 2(a) shows the QD diagram for TPA and relaxation. The TMs are shown in Fig. 3 for absorption and relaxation. Table 2(b) shows the calculated z-scan transmission as a function of z as the solid line (See Fig. 4.) The square dots are the experimental data[26]. This results in a value of 253 cm/GW in close agreement with the published value of 252 cm/GW[26]. The parameters used for the calculation are given in Table 2 (c).

Table 2. 2(a) describes the two-photon absorption and relaxation. 2(b) plots our numerical calculation as a function of z and the experimental data values. 2(c) gives the parameters used for the numerical calculation.

Parameter	Value
I_{00} (GW/cm^2)	3.5
L (cm)	0.00037
w_0 (µm)	85
t_{FWHM} (ps)	25
z_0 (cm)	4.26
λ (nm)	532
N_0(cm^{-3})	5x10^{18}
k_{10}(ps^{-1})	1.0
β (cm/GW)	253
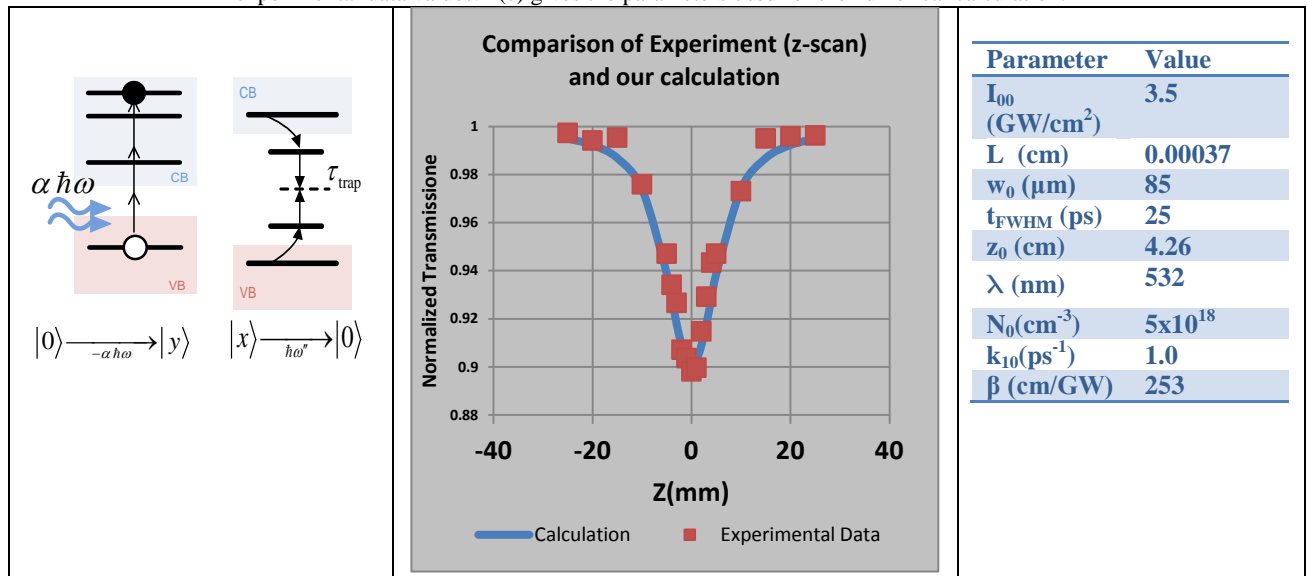
(a)	(b)	(c)

In general analytical calculations[19] of z-scan measurements are used in the plots shown in Table 2(b). However, in addition to calculating the normalized transmission as a function of z, our numerical calculation can also calculate the laser pulse shape at any point through the material as well as the population density of every state. These calculations have an advantage in understanding complex results and predicting physical behavior. Figure 5(a) shows a plot of the pulse intensity as a function of time and radius at z=0 and Fig. 5(b) shows the population of the ground and excited states.

(a)   (b)
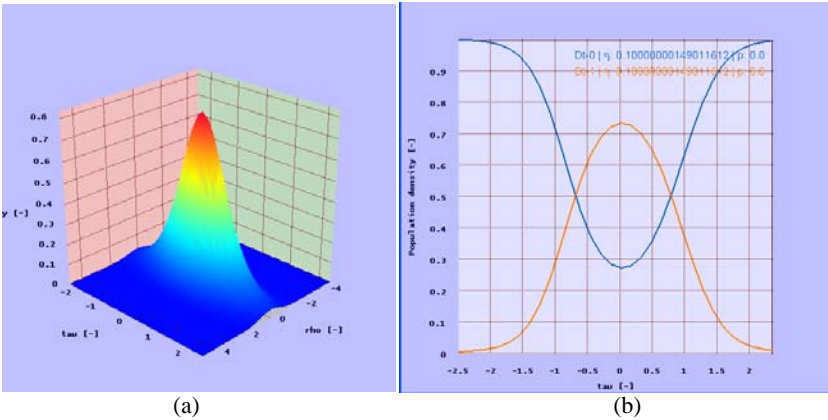
Figure 5. Intensity and population density at z=0. (a) plot of the laser intensity as a function of time and radius (b) population density where the upper (lower) line corresponds to the ground (excited) state.

The two photon absorption parameter obtained for CdS in a surfactant thin film is similar in value to that obtained for CS/ZnS Q-dots[27] also in a thin film where the value obtained was 229 cm/GW. It was assumed that these large values are due to both the quantum confinement and surface modification. Other z-scan measurements have also been obtained for both two-photon as well as three-photon absorptions, a few examples include.[28-,30]

6.2. Two photon absorption in a thick semiconductor QD film with diffraction

We use our numerical method to calculate TPA in a thick semiconductor QD film where diffraction must be taken into account as shown in Table 3.

Table 3. (a) full scale calculation, (b) calculation in the diffraction region, (c) tabulation of the # diffraction lengths and radius

Z cm	# Diff. Length	w(z) (µm)
0	2.343	85
1	2.237	87
2	1.916	94
3	1.565	104
4	1.237	117
5	0.986	131
10	0.359	217
15	0.181	311
20	0.102	408
25	0.066	506
30	0.046	605
Sample length (L) =7cm		

(a)	(b)	(c)

As cited, there have been examples where diffraction has been taken into account[20,22-25]. Yet our method presents a unified way of including diffraction. The parameters are similar to those used in the previous case, except the sample length is 7 cm. Table 3(c) shows the # of diffraction lengths near the focus. At z=0, the beam radius is 85 μm and the # of diffraction lengths is 2.343; while at z=5cm, the radius has increased to 131μm and the # of diffraction length has decreased to 0.986. Fig. 3(a) shows the full z-scan calculation where the arrow indicates the region near the focus shown in Table 3(b). It can be seen that when diffraction is present (dots) the transmission is increased because the light radius increases as it propagates through the material. However as the sample moves away from the focal region, the radius increases and the # of diffraction lengths decreases so that the calculated curves with diffraction (dots) and without (solid line) overlap. The difference in the laser pulse shape at the output of the sample with (peaked line) diffraction and without (flattened line) is shown in Fig. 6(a). Our numerical method can also calculate the population density at every propagation step through the sample which is shown at the output in Fig. 6(b).
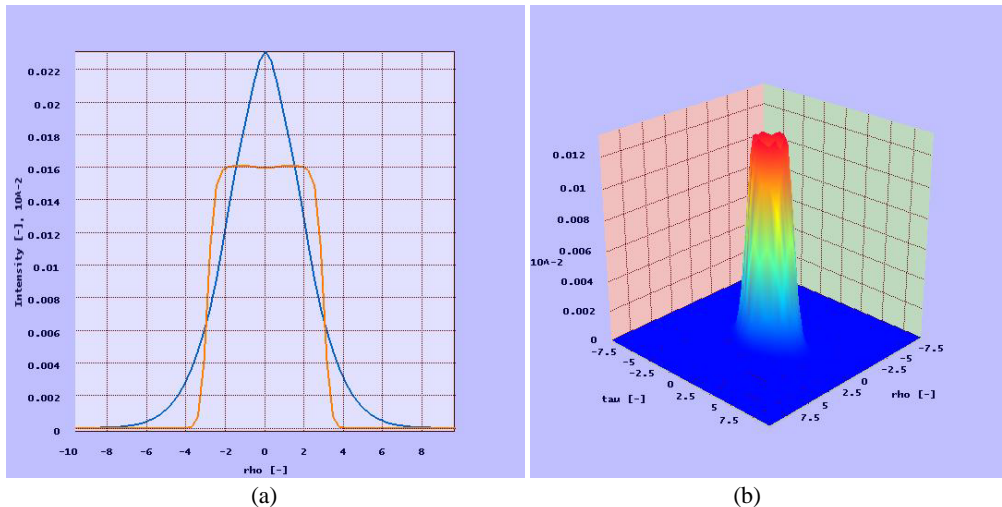

Fig. 6. (a) output pulse shape at z=0 with (peaked line) diffraction and without (flattened line), (b) population density of the excited state at z=0.

6.3 Two-photon absorption and excited state absorption in a semiconductor QD thin film.

In many cases TPA is followed by excited state (ESA) absorption. This situation cannot be calculated with current theories. The z-scan results are shown in Table 4 where (a) shows the transitions involving excitation of TPA and ESA and relaxation, (b) shows the z-scan calculations with (solid line) and without (dashed line) ESA and (c) gives the parameters used in the calculations. For an experimental curve, the values of both TPA and ESA can be obtained using our numerical method.

Table 4. (a) Diagrams showing excitation and relaxation, (b) calculations with (solid line) and without (dashed line) excited state absorption (ESA), (c) parameters used in the calculation.

| (a) | (b) | (c) |
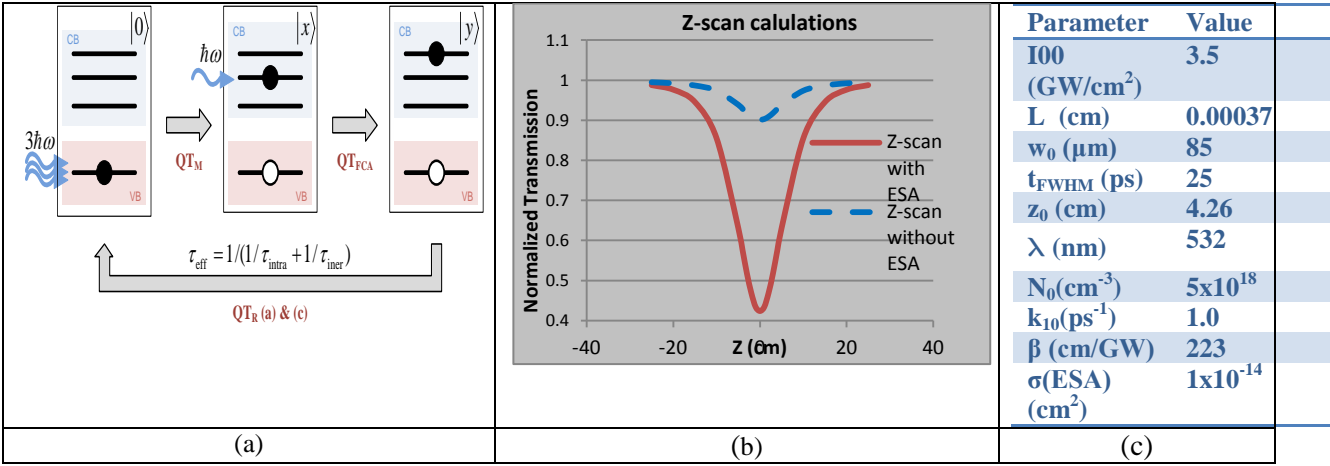
We also calculate the pulse shape as the laser propagates through the sample and the population density of each level in Fig. 7. The pulse intensity as a function of time are shown in Fig. 7(a) where the highest curve is the incident pulse, the next highest curve is at the half-way distance through the material and the lowest curve is at the output of the material. Figure 7(b) shows the population of each level where the upside down curve shows the population depletion of the ground state, the higher upright curve shows the population on the ESA level and the flattened curve shows the population on the TPA level.
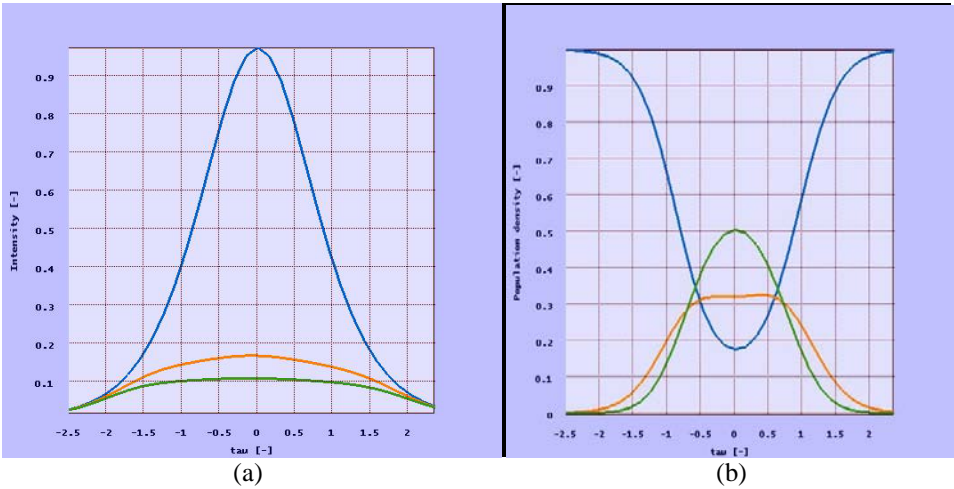

Fig. 7. (a) pulse intensity as a function time, (b) population density of ground state and higher states.

For convenience, Fig. 8 shows calculations of the population density of each level as a function of radius and time. The plots show that both TPA and ESA states are populated.
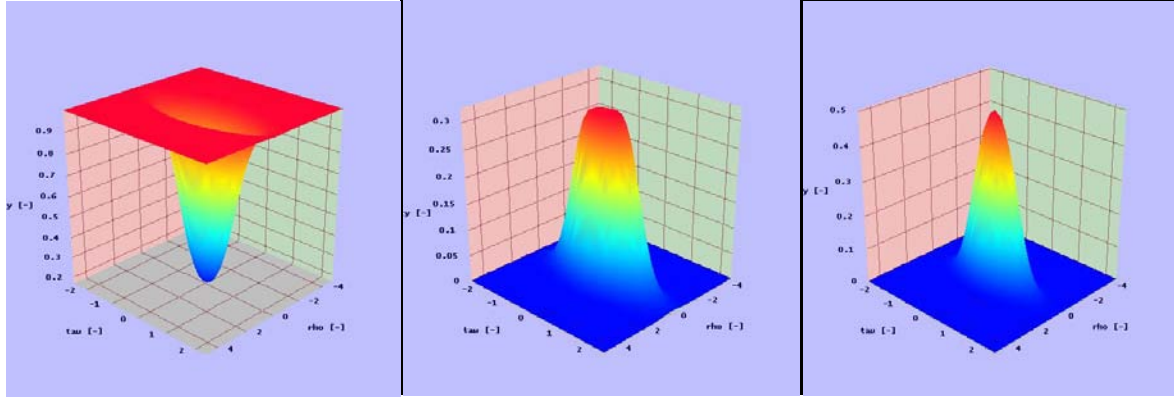
Fig. 8. Population as function of radius and time. Left-ground state, middle-TPA state and right-ESA state.

6.4 Two-photon absorption with two-photon stimulated emission and nonradiative relaxation.

We calculate TPA with stimulated TPA-emission and nonradiative relaxation. Table 5 (a) shows the absorption and relaxation diagrams, (b) calculated populations of ground state and excited state for two incident intensities (left-I=1000 GW/cm^2 and right-3000 GW/cm^2) and (c) parameters used for the calculation.

Table 5. Two-photon absorption with relaxation.

		Parameter	Value
		L (cm)	0.1
		W$_0$ (μm)	60
		t$_{FWHM}$ (fs)	160
		λ (nm)	775
		N$_0$(cm^{-3})	6x10^{18}
		k$_{10}$(ns^{-1})	0.833
		σ(TPA) (cm^4/GW)	5.28e-21
(a)	(b) I= 1000GW/cm^2 I=3000GW/cm^2	σ(TPA_stim emission) (cm^4/GW)	5.28e-21
		(c)	

In Table 5(b), we plot the population as a function of radius for two incident intensities; namely, I=1000GW/cm^2 and I=3000GW/cm^2. The TPA coefficient is 5.28 x 10^{-21} cm^4/GW and the spontaneous decay rate is 0.833ns^{-1}. The calculations assumed a pulse width of t$_{FWHM}$=160fs at a wavelength of 775nm. Calculations at low intensity showed TPA and relaxation; however, the population of the excited state was very small. We demonstrate the population calculations at higher intensity. It can be seen from Table 5(b) that for I=1000GW/cm^2, there is significant population of the excited state in the presence of stimulated and spontaneous emission. The downward pointing curve in Table 5(b) corresponds to the ground state and the upward pointed curve corresponds to the excited state. Saturation (50% population on both ground and excited state) occurs at I=3000GW/cm^2.

The intensity of the pulse as a function of radius and time near saturation is shown in Fig. 9. The figure shows the decrease in intensity near saturation.
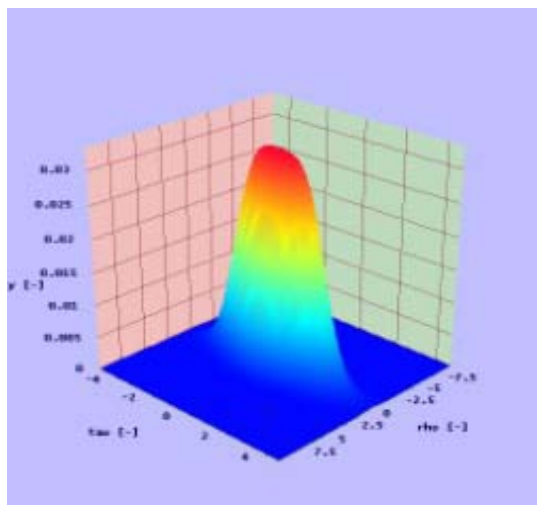
Fig. 9. Intensity as a function of radius and time.

7. SUMMARY

In this paper we have extended and demonstrated our optical building block/transition module methodology for describing existing and/or composing novel energy level diagrams and for building a mathematical model (numerical algorithm) of ultrashort laser interaction with semiconductor quantum dot materials. The method includes diffraction in a unified way. Calculations on semiconductor quantum dots in a thin film agreed very well with experiments and published results. Additionally we calculated z-scan results for thick materials when the number of diffraction lengths exceeded one. Then we calculated novel cases that included additional nonlinear effects such as excited state absorption and stimulated emission demonstrating the versatility of our method.

8. REFERENCES

[1] Brus,L., "Quantum crystallites and nonlinear optics", Appl. Phys.A, 53, 465 (1991).
[2] Efros,Al. and Efros,A., "Interband absorption of light in a semiconductor sphere", Sov. Phys. Sem., 16, 772 (1982).
[3] Alivisatos,A., "Semiconductor clusters, nanocrystals and quantum dots", Science, 271, 933 (1996).
[4] Fendler,J.H., Dekany,I. eds, Nanoparticles in Solids and Solutions], Kluwer Academic Publishers, Boston, (1996).
[5] Gubin,S. P.,Kataeva,N. A. and Khomutov,G. B., Russian Chem Bull, Int. Ed., 54, 827 (2005).
[6] Efros,Al.,Rosen,M., "The electronic structure of semiconductor nanocrystals", Annu. Rev. Mater. Sci., 30, 475 (2000).
[7] Klimov,V.,Mikhallovsky, A.A, McBranch,D.W., Leatherdale, C.A., Bawendi,M.G.,"Quantization of multiparticle Auger rates in semiconductor quantum dots," Science, 287, 1011 (2000).
[8] Alivisatos,A.P., "Perspectives on the physical chemistry of semiconductor nanocrystals", J. Phys. Chem., 100, 13226 (1996).
[9] Parilov,E.,Potasek,M. J., "Generalized theoretical treatment and numerical method of time- resolved radially dependent laser pulses interacting with multiphoton absorbers", J. Opt. Soc. Am., 23, 1894 (2006).
[10] Potasek,M.J., McLaughlin,D.W., Parilov, E., "Optical pulse interactions in nonlinear excited state materials", NASA STAR, Scientific and Technical Reports, 22, 104 (2008).
[11] Parilov,E. and Potasek, M., "Method, system and software arrangement for determining an interaction between a light source and a material" issued patent, 7,949,480 B2, (2011).
[12] Parilov,E., Potasek,M. and Beeson,K. "Determining the interaction between electromagnetic radiation and a material by utilizing transition modules", pending- patent, 2010/0037173 A1, (2010).

[13] He,J., Mi,J., Li,H.and Ji,W., "Observation of interband two-photon absorption saturation in CdS nanocrustals", J. Phys. Chem. B 109, 19184 (2005).
[14] Dumke,W., "Quantum theory of free carrier absorption", Phys. Rev. 124, 1813 (1961).
[15] Klimov,V. I.,McBranch,D. W. "Auger-process-induced charge separation in semiconductor nanocrystals", Phys. Rev. B 55, 13173 (1997)
[16] Klimov,V. I., Mikhailovsky,A.A., Xu,S., Malko,A., Hollingsworth,J.A., Leatherdale,C.A. Eisler,H.J., Bawendi,M. G., "Optical gain and stimulated emission in nanocrystral quantum dots" Science 290, 314 (2000).
[17] Nozik,A.J., "Quantum dot solar cells", Physica E 14, 115 (2002).
[18] Sheik-Bahae,M., Said,A. A., Wei,T., Hagan,D. J. and Van Stryland,E. W., ''Sensitive measurement of optical nonlinearities using a single beam,'' IEEE J. Quantum Electron. 26, 760 (1990).
[19] Van Stryland,E.W. and Sheik-Bahae,M. in Characterization Techniques and Tabulations for Organic Nonlinear Materials, Kuzyk,M. G. and Dirk,C. W., eds., page 655-692, Marcel Dekker, Inc., (1998).
[20] Zang,Wei-Ping,Tian,Jian-Guo, Liu,Zhi-Bo, Zhou,Wen-Yuan, Song,Feng, Zhang,Chun-Ping, "Analytic solutions to z-scan characteristics of thick media with nonlinear refraction and nonlinear absorption", J. Opt. Soc. Am. B, 21, 63 (2004).
[21] Kvosh,D. I., Yang,S.,Hagan,D. J.,Van Stryland,E. W., ''Nonlinear optical beam propagation for optical limiting,''Appl. Opt., 38, 5168 (1999).
[22] Tian, J.-G,. Zang, W.-P. and Zhang, G.-Y., ''Analysis of beam propagation through thick nonlinear media by the variational approach,'' Acta Phys. Sin,. 43, 1712–1717 (1994).
[23] Hermann, J. A. and McDuff, R. G. ''Analysis of spatial scanning with thick optically nonlinear media,'' J. Opt. Soc. Am.B 10, 2056–2064 (1993).
[24] Tian, J.-G,. Zang, W.-P., Zhang, C.-Z. and Zhang, G.-Y.,''Analysis of beam propagation through thick nonlinear media,''Appl. Opt,. 34, 4331–4336 (1995).
[25] Chapple, P. B., Staromlynska, J. and. McDuff, R. G, ''Z-scan studies in the thin- and the thick-sample limits,'' J. Opt.Soc. Am. B, 11, 975–982 (1994).
 [26] Gao, Y.,Tonizzo,A.,Walser,A.,Potasek, M. and Dorsinville,R., "Enhanced optical nonlinearity of surfactant-capped CdS quantum dots embedded in an optically transparent thin film", Appl. Phys. Lett.,92, 033106 (2008).
[27] Wang, X.,Du,Y., Ding,S., Fan,L., Shi, X., Wang, Q., Xiong, G., "Large two-photon absorbance of chitosan-ZnS quantum dots nanocomposite film", Physica E, 30, 96 (2005).
[28] He, J., Mi,J., Li,H., Ji, W., "Observation of interband two-photon absorption saturation in CdS nanocrystals", J. Phys. Chem. B, 109,19184 (2005).
[29] He, J., Qu, Y., Li, H., Mi,J. ,Ji, W., "Three-photon absorption in ZnO and ZnS crystals", Opts. Exp. 13, 9235 (2005).
[30] Chon, J.W.,Gu,M., Bullen,G., Mulvaney,P., "Three-photon excited band edge and trap emission of CdS semisonductor nanocrystals", Appl. Phys. Let, 84, 4472 (2004).